PCCP

Accepted Manuscript

ROYAL SOCIETY OF CHEMISTRY

www.rsc.org/pccp

PCCP

RSCPublishing

ARTICLE

Synthesis of Rare Earth Doped Yttrium-Vanadate nanoparticles Encapsulated with Apoferritin

Cite this: DOI: 10.1039/x0xx00000x

Tomoaki Harada and Hideyuki Yoshimura*

Received 00th January 2012,
Accepted 00th January 2012

DOI: 10.1039/x0xx00000x

www.rsc.org/

Luminescent europium (Eu) and dysprosium (Dy) doped Yttrium-Vanadate (Y-V) nanoparticles (NPs) were synthesized in a cavity of the protein, apoferritin. Y-V NPs were synthesized by incubating a solution of apoferritin with Y^{3+} and VO_3^- ions in the presence of ethylene diamine-N-N′-diacetic acid (EDDA). EDDA plays an important role in preventing Y-vanadate precipitation in bulk solution by chelating the Y^{3+} ions. Using high resolution electron microscopy, the obtained NPs in the apoferritin cavities were confirmed to be amorphous, and to consist of Y and V. Eu-doped Y-V (Y-V:Eu) NPs were synthesized by the same procedure as Y-V NPs, except that $Eu(NO_3)_3$ was added. Y-V:Eu NPs exhibited a strong absorption peak due to the O-V charge transfer transition and remarkable luminescence at 618 nm due to the $^5D_0 \rightarrow {}^7F_2$ transition. The luminescence lifetime of Y:Eu and Y-V:Eu NPs measured in H_2O and D_2O solution showed reduction of non-radiative transition to the O-H vibration in Y-V:Eu NPs. Accordingly, Y-V NPs showed strong luminescence compared to Y:Eu NPs. Dy-doped Y-V NPs were also synthesized in apoferritin cavities and showed luminescence peaks at 482 nm and 572 nm, corresponding to $^4F_{9/2} \rightarrow {}^6H_{15/2}$ and $^4F_{9/2} \rightarrow {}^6H_{13/2}$ transitions. These NPs stably dispersed in water solution since their aggregation was prevented by the protein shell. NPs encapsulated in protein are likely to be biocompatible and would have significant potential for biological imaging applications.

Introduction

Molecular labeling is an important technique for medical applications as well as for basic research in molecular biology. Organic fluorescent dyes are usually used for this purpose. However, these classical fluorescent dyes bleach easily due to degradation caused by irradiation with excitation light. The use of inorganic nanoparticles (NPs) in place of organic dyes is becoming increasingly widespread for molecular labeling because of their strong resistance to photobleaching.[1] These NPs are commonly synthesized in organic solvent at high temperature, but the products have poor water solubility. To improve water solubility, it is necessary to coat the surface of the NPs with phospholipids or hydrophilic polymers.[1] Protein can be also utilized as a shell around the NP to prevent aggregation. Apoferritin is a hollow, spherical protein and is known to accumulate metal ions in its cavity and form NPs. As a result, the synthesized NPs have a narrow size distribution and are stably dispersed in water solution.[2, 3] For these reasons, apoferritin has been investigated for synthesizing luminescent NPs of II-VI semiconductor (CdS[4, 5], CdSe[6, 7] and ZnSe[8]) within the apoferritin cavity, as recently reported. Crystallinity of the NPs is very important for obtaining luminescent semiconductors with high quantum yield, however in our experience, it is difficult to obtain well-ordered nanocrystals in the apoferritin cavity, and consequently luminescence is very weak. In contrast to these luminescent NPs, luminescence from rare earth ions is less influenced by environmental conditions because emission occurs due to the transition within the f-orbitals of the ion itself and thus is screened by the outer orbitals. We have reported the synthesis of Y-based Eu- and Tb-doped NPs in the apoferritin cavity, however, the luminescence intensity of the NPs was insufficient for imaging purposes.[9] One reason is the non-radiative transition of the excited state of the ions to higher frequency vibration of the O-H bonds.[10, 11] To address this, rare earth ion-doped Y-vanadate was investigated. In addition, Y-V NPs show a higher molar extinction coefficient in the UV region due to the O-V charge transfer effect[12, 13]; consequently, Y-V NPs exhibit stronger luminescence than Y- based NPs. Here, we describe the synthesis of Eu- and Dy-doped Y-V NPs encapsulated with apoferritin which exhibit high luminescence. Since the structure of protein is strictly regulated by DNA, the size of NPs also becomes homogeneous. Particularly apoferritin is thermally stable water soluble protein, thus encapsulated NPs are also stably dispersed in aqueous solution. In addition to these merits using protein cage for NPs synthesis, the sequence of a protein can be modified by protein engineering to enable the protein to bind to a specific molecule,[14, 15] *e.g.* an aptamer, these NPs have significant potential for biological imaging.

Experimental

Materials

Recombinant apoferritin cloned from horse liver L-apoferritin was used throughout the experiments. Recombinant L-apoferritin (fer0) was expressed in *E. coli* and purified, as reported previously.[16] 3-Morpholinopropanesulfonic acid (MOPS), N-(1-1-dimethyl-2-hydroxyethyl)-3-amino-2-hydroxypropanesulfonic acid (AMPSO), yttrium nitrate hexahydrate ($Y(NO_3)_36H_2O$), and heavy water (D_2O) were obtained from Sigma-Aldrich. Europium nitrate hexahydrate ($Eu(NO_3)_36H_2O$) was purchased from Strem Chemicals. Ammonium vanadate (NH_4VO_3), dysprosium nitrate hexahydrate ($Dy(NO_3)_36H_2O$), and aurothioglucose were purchased from Wako Pure Chemical Industries, Inc. Ethylene diamine-N-N′-diacetic acid (EDDA) was purchased from Tokyo Chemical Industry, Co. A staining reagent, Nano-W, was obtained from Nanoprobes, Inc.

Methods

Y NPs and Eu-doped Y NPs (Y:Eu) encapsulated in apoferritin (fer0) were prepared by the method reported previously.[9] Nanoparticle formation in the apoferritin cavity was confirmed by transmission electron microscopy (TEM; JEM1200EX, JEOL) by staining samples with 2% aurothioglucose or Nano-W. These staining reagents do not penetrate into the apoferritin cavity. The fine structure and elemental composition of the NPs were investigated by high-resolution TEM (HRTEM; JEM2100F, JEOL) at 200 kV without staining. The nanoparticle formation ratio (NFR), which was calculated by dividing the number of apoferritin-containing NPs (holoferritin) by the total number of apoferritin molecules, was estimated from TEM images of aurothioglucose stained samples. The elemental compositions of the NPs were determined by energy dispersive X-ray spectroscopy (EDX) using the scanning transmission mode of the HRTEM. The content ratios of V, Y, Eu, and Dy were estimated from the intensity of the Kα or Lα lines of characteristic X-rays of each element using the intensity of standard samples as references. The elemental composition of the NPs was also examined by an inductively coupled plasma optical emission spectrometry (ICP-OES; SII NanoTechnology Inc., SPS4000). Purified holoferritin samples were dissolved in concentrated nitric acid and were 100 times diluted to 2 mL for ICP analysis.

To separate holoferritin from empty apoferritin molecules, the obtained solution containing holoferritin was subjected to sucrose density gradient centrifugation as reported before.[9] Using this procedure, we obtained holoferritin with a nanoparticle formation ratio (NFR) of nearly 100%.

The NPs for luminescence measurement were purified by sucrose density centrifugation. The sucrose was subsequently removed by gel-filtration chromatography (G25). The NPs were then concentrated using a centrifugal filter device (Amicon Ultra 50k). Photoluminescence was measured using a spectrofluorometer (JASCO, FP-6200) with a microfluorometer cell. The luminescence lifetime was measured with a TemPro spectrofluorometer (Horiba, Ltd.) equipped with a Spectra LED-390 pulsed light source (390 nm excitation wavelength).

Result and Discussion

Preparation of Y-V NPs

Previously we reported the synthesis of Y NPs in apoferritin cavities by adding 1 mM $Y(NO_3)_3$ solution into 0.1 mg/mL apoferritin in 100 mM MOPS (pH 7.0) solution.[9] To synthesize Y-V NPs in the apoferritin cavity, we used a similar procedure, incubating 0.1 mg/mL apoferritin in 3 mM $Y(NO_3)_3$, 3 mM NH_4VO_3 and 100 mM MOPS (pH 7.0). However this solution rapidly became cloudy and formed a white precipitate of Y-V compound. To prevent the rapid chemical reaction between Y and V ions, a chelating agent, EDDA, was used to keep Y^{3+} ions at a low concentration. The chelating agent could not penetrate the apoferritin ion channel, so the concentration of Y^{3+} ions accumulated in the apoferritin cavity was higher than the concentration outside the apoferritin molecule. A similar strategy to prevent a rapid chemical reaction was used to synthesize a CdSe nanoparticle in the apoferritin cavity.[6, 7] To determine the optimum conditions for NP synthesis, EDDA concentrations between 0 to 100 mM were tested. A 10 mL solution of EDDA, 3 mM $Y(NO_3)_3$, 0.1 mg/mL apoferritin, and 100 mM MOPS (pH 7.0) was incubated at 4 °C, then 46.8 mg of NH_4VO_3 was gradually added. The mixture was incubated for 24 hours with gentle stirring at 4 °C. The resultant solution was then centrifuged for 20 minutes at 10,000 × g to remove the precipitant. The supernatant was applied to a gel-filtration chromatography (Sephadex G-25 Fine, GE Healthcare) column to remove free metal ions and EDDA. The nanoparticle formation ratio (NFR) at various EDDA concentrations is shown in Fig. 1. The NFR showed a maximum value of 12% at 30 mM EDDA, whereas no NPs were found using 0 mM and 100 mM EDDA. An aurothioglucose-stained TEM image of the NPs obtained at a concentration of 30 mM EDDA is shown in Fig. 2a. As shown in the inset of Fig. 2a, no lattice structures in the NPs were observed. Following size-

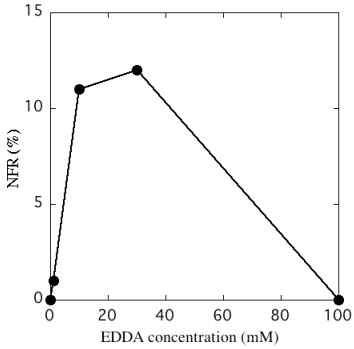

Fig.1 NFR at different EDDA concentration.NFR (nanoparticle formation ratio) was determined using aurothioglucose-stained TEM images.

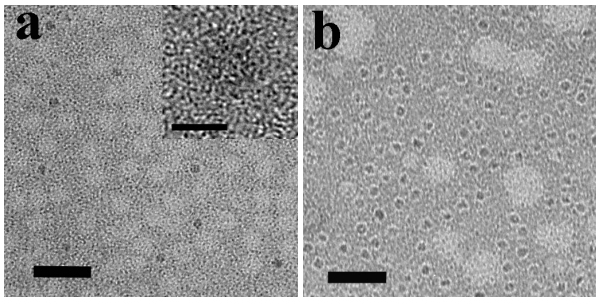

Fig.2 Aurothioglucose-stained TEM images of Y-V NPs in apoferritin. (a) TEM image of Y-V NPs at 30 mM EDDA concentration (NFR=12%). The white disks correspond to apoferritin protein, and the dense dots with white rings correspond to apoferritin with NPs. The inset is an HRTEM image of a nanoparticle showing its amorphous structure. Scale bar indicates 5 nm. (b) TEM image of Y-V NPs after sucrose gradient centrifugation. The NFR was improved to nearly 100%. Scale bars for (a) and (b) indicate 50 nm.

exclusion chromatography, the solution was subjected to sucrose gradient centrifugation and the holoferritin was collected (Fig. 2b). The average size of the obtained NPs was 6.6 ± 0.7 nm. EDX showed that the NPs consist of Y and V (Fig. 3). The molar ratio of Y:V was about 6:4 under this condition. The chemical structure of the NPs is unclear, as the NPs are amorphous, however, the NPs likely contain some form of vanadate. The absorption spectrum of Y-V NPs shows a strong absorption peak at 274 nm due to O-V charge transfer transition[12]; this absorption peak was not observed in Y-NPs (Fig. 4).

The concentration of free Y^{3+} at 30 mM EDDA and 3 mM $Y(NO_3)_3$ was calculated to be about 3 μM at pH 7.0, assuming that the acid dissociation constants of EDDA are pK_{a1}=6.59 and pK_{a2}=9.58, and that the complex formation constant (K_{ML}) of EDDA with Y^{3+} is 6.78. The solubility product of Y-V salt formation is not clear, however 3 μM Y^{3+} would be sufficiently low to prevent rapid precipitation of Y-V salt in the bulk solution. Because of the negative electrostatic potential in the

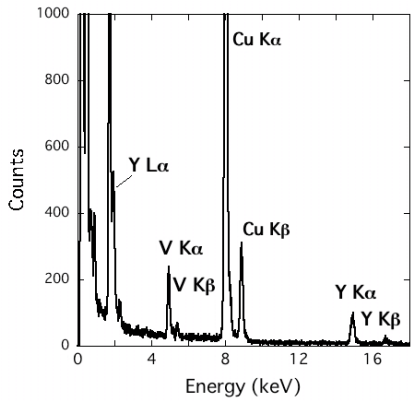

Fig. 3 EDX of Y-V NPs. The purified specimen was investigated by EDX. Specific peaks were detected for Y (Lα (1.92 keV), Kα (14.9 keV), Kβ (16.7 keV)) and for V (Kα (4.95 keV), Kβ (5.43 keV)). Cu peaks (Kα (8.05 keV), Kβ (8.91 keV)) originate from the specimen grid. The molar content ratio in this case is calculated to be Y:V=6:4.

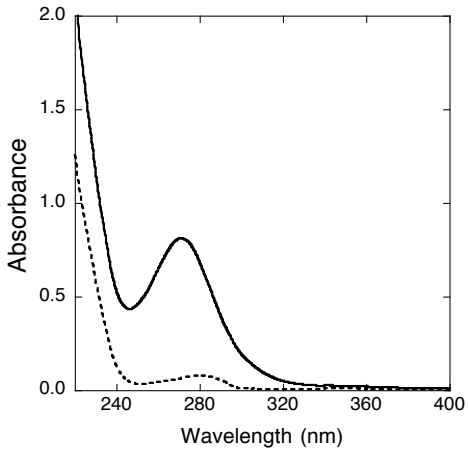

Fig. 4 Absorption spectra of Y NPs and Y-V NPs. Absorption spectra were obtained from purified 0.1 mg/mL holoferritin (NFR≈100%) solution. An absorption peak due to the O-V charge transfer transition was observed at 274 nm in Y-V NPs (continuous line), but it was not observed in Y NPs (broken line). A weak absorption peak at 280 nm in Y NPs is due to apoferritin aromatic amino acid groups.

apoferritin cavity,[17] Y^{3+} accumulates in the apoferritin cavity, so its concentration becomes higher in the cavity than in the bulk solution. Cations would neutralize negative charges in the cavity, and then VO_3^- anion would diffuse into the cavity to form the Y-V complex. The pathway of cations into apoferritin cavity is thought to be the three fold symmetry channel which is rich in basic amino acids, however that of anions is not clear. Since electrostatic potential gradient at the four fold symmetry channels of apoferritin is directed toward outside from inside the molecule,[18] anions may path through this channels. NPs did not form when NH_4VO_3 was incubated without Y^{3+} ion, indicating that the presence of a cation is required for the formation of a nanoparticle in an apoferritin cavity.

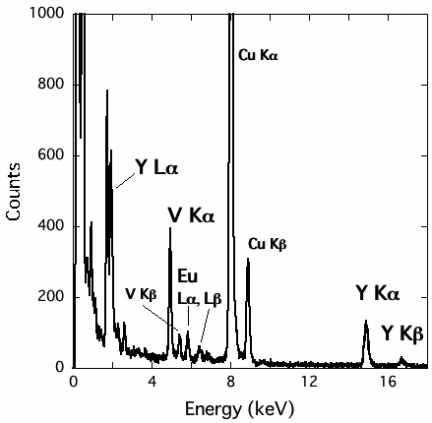

Fig.5 EDX of Y-V:Eu NPs. Purified Y-V NPs (Eu content 11.5%) were investigated by EDX. Specific peaks were detected for Y (Lα (1.92 keV), Kα (14.9 keV), Kβ (16.7 keV)), for V (Kα (4.95 keV), Kβ (5.43 keV)), and for Eu (Lα (5.84 keV), Lβ (6.46 keV)). Cu peaks originate from the specimen grid.

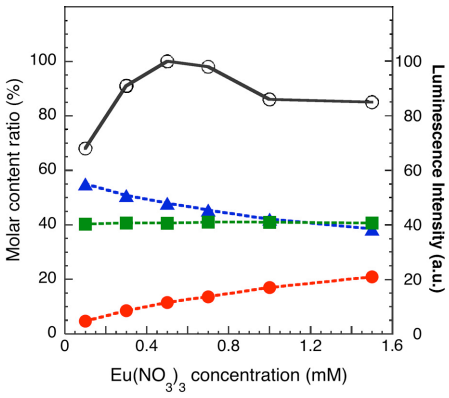

Fig.6 Content ratio of Y, V, and Eu in Y-V:Eu NPs and luminescence intensity. The content ratio of Eu (red closed circles, broken line), V (green closed squares, broken line) and Y (closed blue triangles, broken line) in NPs against the initial $Eu(NO_3)_3$ concentration was examined by ICP-OES. The ratios were calculated so that [Y]+[V]+[Eu]=100. The V content was constant at all $Eu(NO_3)_3$ concentrations. The luminescence intensity normalized by maximum intensity was plotted against the initial $Eu(NO_3)_3$ concentrations (open black circles, continuous line).

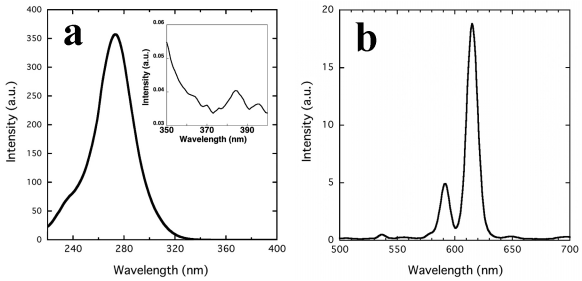

Fig. 7 Luminescence spectra of Y-V:Eu NPs. (a) Excitation spectrum (615 nm emission) of 11.5% Y-V:Eu NPs. A significant peak at 274 nm due to the O-V charge transfer transition was observed. Inset is the wavelength-expanded spectrum between 350 nm to 400 nm. Weak peaks at 384 nm and 395 nm due to f-f transitions were also observed. (b) Emission spectrum (excitation at 274 nm) of 11.5 % Y-V:Eu NPs. Intense peaks at 614 nm and 590 nm correspond to the transitions $^5D_0 \rightarrow {}^7F_2$ and $^5D_0 \rightarrow {}^7F_1$ of Eu^{3+} were observed.

Preparation of Eu-doped Y-V (Y-V:Eu) NPs

Eu-doped Y-V NPs were synthesized by the same procedure as Y-V NPs with 30% EDDA except that $Eu(NO_3)_3$ was added together with $Y(NO_3)_3$. Concentrations of $Eu(NO_3)_3$ between 0.1 mM to 1.5 mM were tested. Each resultant solution was purified and concentrated by sucrose gradient centrifugation as described in the previous section. NPs were found to form in the apoferritin cavity at all Eu concentrations. These NPs were amorphous and did not have a lattice structure. EDX showed that the NPs contain Y, V, and Eu (Fig. 5). The ratio of these elements in the NPs compared to the initial $Eu(NO_3)_3$ concentration was examined by ICP-OES (Fig. 6). Since the content of V was held constant as the Eu concentration changed, Y would be substituted with Eu as the Eu concentration increased. The luminescence intensity was maximum at Eu content of 11.5% (Fig. 6), which is much higher than the concentration observed in the bulk solution. Concentration quenching reduces the luminescence intensity at higher concentration of doped Eu; however, this quenching would be insignificant for nano-scale particles dispersed in the solution.

Because no lattice structure was observed in the Y-V:Eu NPs, the chemical structure of the NPs is unclear. However it is likely that Y and Eu are coordinated by vanadate. Y-V nanoparticles encapsulated in apoferritin were found to be stable when diluted into a neutral pH (pH=7) solution, whereas encapsulated Y NPs dissolved into the bulk solution under these conditions.[9]

Optical properties of Eu-doped V-Y (Y-V:Eu) NPs

The excitation spectrum of purified and concentrated Y-V:Eu NPs at 615 nm ($^5D_0 \rightarrow {}^7F_2$ transition) is shown in Fig. 7a. The spectrum showed a significant peak at 274 nm due to the O-V charge transfer transition.[12] Small peaks at 384 nm and 395 nm, due to f-f transitions, were also observed (Inset of Fig. 7a). The emission spectrum of Y-V:Eu NPs excited at 274 nm is shown in Fig. 7b. The emission peaks observed at 614 nm and 590 nm correspond to the transitions $^5D_0 \rightarrow {}^7F_2$ and $^5D_0 \rightarrow {}^7F_1$ of Eu^{3+}, respectively. It is known that the $^5D_0 \rightarrow {}^7F_1$ transition mainly originates from the magnetic dipole transition and is not sensitive to the environment of the Eu^{3+}. In contrast, the $^5D_0 \rightarrow {}^7F_2$ transition is assigned to the electric dipole transition and is suppressed when the Eu^{3+} ion is in a symmetric position.[19] In NPs encapsulated in apoferritin, the Eu^{3+} ions are believed to be positioned in an asymmetric site, as in Eu-doped Y_2O_3 crystals.

The luminescence lifetime observed at 615 nm emission (excitation at 390 nm) was measured for Y:Eu and Y-V:Eu NPs in water (H_2O) solution. The lifetime vs. several Eu concentrations is presented in Fig. 8, and several typical decay curves are shown in Fig. 9. The decay curve of Y:Eu NPs in water solution fit well to a single exponential decay, whereas the other decay curves required two components for fitting. The lifetime was slightly reduced as the Eu concentration was increased due to concentration quenching; however, quenching was not as significant as in the bulk sample because the particle size was nanometer scale.[13] The lifetime of the fast decay component of V-Y:Eu NPs was almost the same as the lifetime of Y:Eu NPs.

Contribution of non-radiative transition of Eu^{3+} excited state to O-H vibration

To investigate the non-radiative transition pathway of Y:Eu and Y-V:Eu NPs, the lifetime of these NPs in water (H_2O) and heavy water (D_2O) were compared. It is known that high frequency O-H vibrations play a dominant role in the non-radiative transition from excited Eu^{3+} ions. Because the vibration frequency of O-D is about 70% that of O-H, this non-radiative transition is suppressed in D_2O solution.[10] The lifetime (τ) of Y:Eu and Y-V:Eu NPs in D_2O vs. Eu concentration is plotted in Fig. 8, and typical decay curves are shown in Fig. 9.

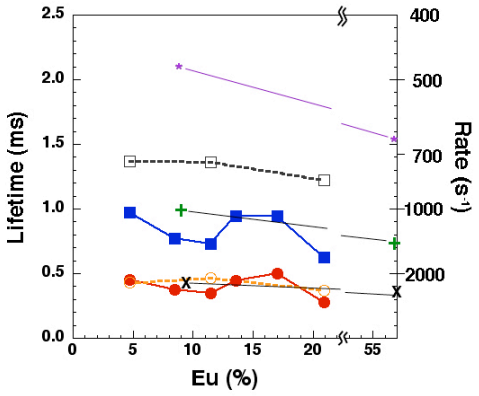

Fig.8 Lifetime of Y:Eu and Y-V:Eu nanoparticles in H_2O and D_2O. The fast decay component (closed circle, red) and slow decay component (closed square, blue) of Y-V:Eu in water (H_2O) was plotted and shown as a solid line. The fast decay component (open circle, orange) and slow decay component (open square, black) of Y-V:Eu in heavy water (D_2O) was plotted and shown as a broken line. The decay curve for Y:Eu NPs in H_2O was fit with a single exponential and is marked by "X" (black solid line). The fast decay component (+, green solid line) and slow decay component (*, purple solid line) of Y:Eu in D_2O was plotted as a solid line.

In general, the transition rate constant (k=1/τ) for the relaxation of the excited state can be expressed as the sum of the different quenching contributions. It is known that quenching through O-H vibration is dominant in rare earth ions; thus, the resultant rate constant k in water solution may be expressed as follows:

$$k = k_{Eu} + k_{nr} + k_{EuEu} + k_{OH}$$

where k_{Eu} is the intrinsic relaxation rate constant of excited Eu^{3+}, k_{OH} is the rate constant for energy transfer to the O-H vibrations of coordinated hydroxyl groups, and k_{nr} is the sum of other non-radiative transitions. The value k_{EuEu} represents the effect of concentration quenching. In the case of a protein-encapsulated nanoparticle, one more term may be required: k_{prt}, which represents quenching through the protein molecule. This means that there are two environmental conditions associated with Eu^{3+}: one is the interaction with protein ($k_p = k_{Eu} + k_{nr} + k_{EuEu} + k_{prt}$) and the other is independent of the protein ($k_i = k_{Eu} + k_{nr} + k_{EuEu} + k_{OH}$). Because the decay observed in Y:Eu NPs is fit by a single exponential, k_p would be equal to k_i, and the rate of k_{OH} and k_{prt} will be similar. Consequently, k_p and k_i can be estimated from Fig. 8 to be approximately 2200 s^{-1} (0.45 ms). The k_{OH} will be also be suppressed strongly when Eu^{3+} is coordinated by vanadate. For this reason, a slow decay component appeared in Y-V:Eu NPs while k_p was unchanged. This effect also will occur when Eu^{3+} is coordinated by O-D. Due to the reduction of k_{OH}, a slow component appeared for Y-V:Eu nanoparticles in D_2O solution, whereas the rate of the fast component (k_p) remained unchanged. However, the decay of Y:Eu in D_2O was observed as two components (about 500 and 1000 s^{-1}) and did not contain any component around 2200 s^{-1}. This may be explained by the instability of the Y:Eu nanoparticle in apoferritin. The Y:Eu nanoparticles easily dissolved into the bulk solution at neutral pH, indicating that protein-nanoparticle interactions may be weaker than in Y-V:Eu NPs.

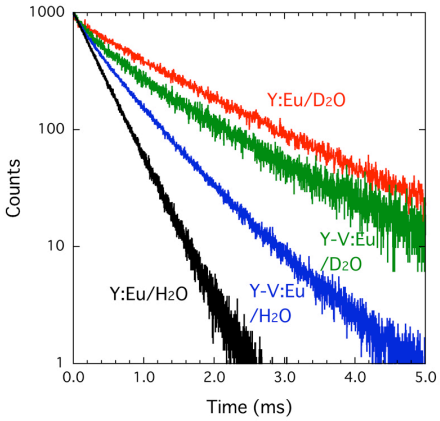

Fig. 9 Luminescence decay curve of Eu-doped NPs. The decay curve of Y:Eu NPs in water solution (black) fit well to a single exponential decay, whereas the other decay curves required two components. The decays of Y-V:Eu in water, Y-V:Eu in heavy water, and Y:Eu in heavy water are represented as blue, green, and red curves, respectively.

If it is assumed that not all O-H oscillators contribute to relaxation in heavy water, the difference in the rate constant (Δk) in water (k_{H2O}) and heavy water (k_{D2O}) can be related to the number of coordinated O-H oscillators (q):[11]

$$q = A\Delta k = A(k_{H2O} - k_{D2O})$$

where A is the proportionality constant. A was experimentally determined to be 1.2 ms for the Eu ion. In the case of Y:Eu, decay was a single exponential in H_2O, while it was a double exponential in D_2O. Nevertheless, if the average rate constant is used for the calculation (620 and 750 s^{-1} for 9 and 57% Eu concentration, respectively), then Δk is about 2000 s^{-1} and q is calculated to be about 2. This number is much smaller than the value of q calculated for free Eu ion ($Eu(NO_3)_3$ solution), which is about 10 (data not shown). In the case of Y-V:Eu, using the slow component of the transition rate, q is calculated to be between 0.3 to 0.8, a coordination number that is smaller than that of Y:Eu.

Because of the suppression of non-radiative transition by the coordinating vanadate, and also because of the strong O-V charge transfer process, the luminescence intensity of Y-V:Eu NPs upon UV excitation was much higher than that of Y:Eu NPs. Strong red luminescence was easily observed by eye, even in a brightly lit room (Fig. 10).

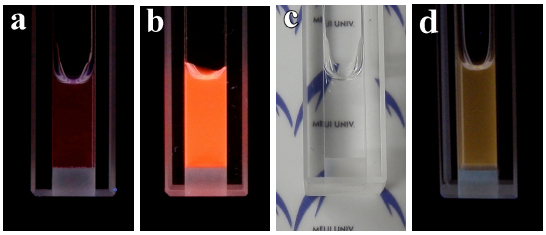

Fig. 10 Luminescence of Y:Eu, Y-V:Eu, and Y-V:Dy NPs. Luminescence was observed by excitation at 254 nm with a UV lamp. The concentration of apoferritin in the microfluorometer cell was 1 mg/mL (NFR≈100%) in each sample. (a) Y:Eu NPs, (b) Y-V:Eu NPs, (c) Same sample as (b) in room light. The sample was transparent. (d) Y-V:Dy NPs at 254 nm excitation.

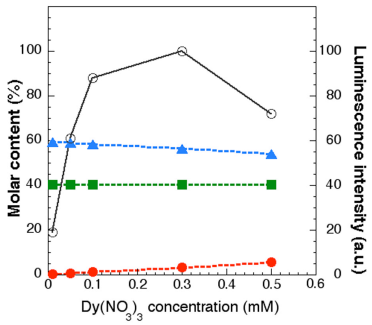

Fig. 11 Content ratio of Y, V, Dy in Y-V:Dy NPs and luminescence intensity. Content ratio of Dy (red closed circles, broken line), V (green closed squares, broken line) and Y (closed blue triangles, broken line) in NPs against initial $Dy(NO_3)_3$ concentration as examined by ICP-OES. The ratios were calculated so that [Y]+[V]+[Dy]=100. The V content was constant at all $Dy(NO_3)_3$ concentrations. The luminescence intensity normalized to the maximum intensity was plotted against the initial $Dy(NO_3)_3$ concentrations (black open circles, continuous line).

Preparation of Dy-doped Y-V (Y-V:Dy) NPs

Dy-doped Y-V NPs were synthesized by the same procedure as Y-V:Eu NPs, except that $Dy(NO_3)_3$ was added instead of $Eu(NO_3)_3$. The concentration of $Dy(NO_3)_3$ was varied from 0.01 mM to 0.5 mM. After purification, the resultant molar content of each element incorporated into the NPs was examined by ICP-OES. The results are shown in Fig. 11 and are similar to Eu doping: the V was kept constant and Y was substituted by Dy by increasing the Dy concentration. The amount of incorporated Dy was less than that of Eu under the same solution conditions. Luminescence showed maximum intensity at a Dy content of 3.4% (Fig. 11). Nanoparticle formation and the elemental composition were confirmed by HRTEM. The NPs were amorphous and showed specific EDX peaks corresponding to Dy, Y, and V.

Optical properties of Dy-doped V-Y (Y-V:Dy) NPs

The excitation spectrum (emission at 572 nm) of purified and concentrated Y-V:Dy is shown in Fig.12a. The spectrum shows a significant peak at 274 nm due to the O-V charge transfer transition. Small peaks at 353, 364 and 388 nm correspond to f-f transitions in Dy^{3+} (Inset of Fig. 12a). The emission spectrum of Y-V:Dy NPs excited at 274 nm is shown in Fig. 12b. The intense emission peaks at 482 nm and 572 nm correspond to the transitions $^4F_{9/2}\rightarrow{}^6H_{15/2}$ and $^4F_{9/2}\rightarrow{}^6H_{13/2}$ of Dy^{3+}. This solution had a yellow color under UV irradiation (Fig. 10d).

We have tested other rare earth elements as dopants in Y-V based NPs. In preliminary experiments, we have succeeded in obtaining luminescent NPs using Tb but failed to obtain Er- and Tm- doped NPs. Further experiments are required to optimize the conditions for their synthesis.

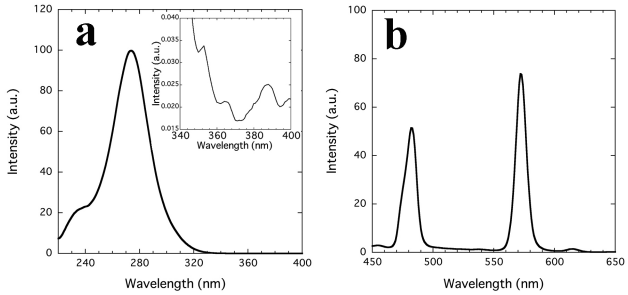

Fig. 12 Luminescence spectra of Y-V:Dy NPs. (a) Excitation spectrum of 3.7% Dy-doped Y-V NPs observed at 572 nm. An intense peak at 274 nm due to O-V charge transfer was observed. Inset is the wavelength-expanded spectrum between 340 nm and 400 nm, showing weak f-f transitions. (b) Emission spectrum (excitation at 274 nm) of 3.7% Dy-doped Y-V NPs. Intense emission peaks at 482 nm and 572 nm corresponding to the transitions $^4F_{9/2}\rightarrow{}^6H_{15/2}$ and $^4F_{9/2}\rightarrow{}^6H_{13/2}$ were observed.

Conclusions

Size-controlled Y-V NPs, Y-V:Eu and Y-V:Dy NPs, which stably dispersed in water solution, were synthesized in apoferritin cavities. The optimum doping concentration was 11.4% and 3.5% for Eu- and Dy-doped Y-V NPs, respectively. These values are much higher than that of the bulk samples because concentration quenching is less effective in nanoparticles.[13]

Compared with Y NPs, luminescence was significantly enhanced in Y-V NPs because of non-radiative transition suppression and efficient energy absorption. However, the effective excitation range is still in the UV region. It would be desirable to shift the effective excitation range to the visible light region for more conventional uses. Other doping materials, as well as optimization of the reaction conditions, are required for further improvements.

Acknowledgements

This study was supported by the Ministry of Education, Culture, Sports, Science and Technology (MEXT) program for the Strategic Research Foundation at Private Universities, 2009–2014.

Meiji University, Department of Physics, 1-1-1 Higashimita, Tama-ku, Kawasaki, 214-8571, Japan.
E-mail: hyoshi@isc.meiji.ac.jp

References

1. M. J. Ruedas-Ramaa, J. D. Waltersb, A. Ortea and E. A. H. Hall, *Analtyca Chemica Acta*, 2012, 751, 1.
2. F. C. Meldrum, V. J. Wade, D. L. Nimmo, B. R. Heywood and S. Mann, *Nature*, 1991, 349, 684.
3. H. Yoshimura, *Colloids Surf. A*, 2006, 282-283, 464.
4. K. K. W. Wong and S. Mann, *Adv. Mater.*, 1996, 8, 928.

5. K. Iwahori and I. Yamashita, *J. Phys.; CS*, 2007, 61, 492.
6. I. Yamashita, J. Hayashi and M. Hara, *Chem. Lett.*, 2004, 33, 1158.
7. R. Xing, X. Wang, L. Yan, C. Zhang, Z. Yang, X. Wanga and Z. Guo, *Dalton Trans.*, 2009, 2009, 1710.
8. K. Iwahori, K. Yoshizawa, M. Muraoka and I. Yamashita, *Inorg. Chem.*, 2005, 44, 6393.
9. T. Harada and H. Yoshimura, *J. Appl. Phys.*, 2013, 114, 044309.
10. J. L. Kropp and M. W. Windsor, *J. Chem. Phys.*, 1965, 42, 1599.
11. A. Beeby, I. M. Clarkson, R. S. Dickins, S. Faulkner, D. Parker, L. Royle, A. S. d. Sousa, J. A. G. Williams and M. Woods, *J. Chem. Soc., Perkin Trans. 2*, 1999, 493.
12. K. Riwotzki and M. Haase, *J. Phys. Chem. B*, 1998, 102, 10129.
13. A. Huignard, T. Gacoin and J.-P. Boilot, *Chem. Mater.*, 2000, 12, 1090.
14. K.-I. Sano, K. Ajima, K. Iwahori, M. Yudasaka, S. Iijima, I. Yamashita and a. K. Shiba, *Small*, 2005, 1, 826.
15. M. Uchida, M. L. Flenniken, M. Allen, D. A. Willits, B. E. Crowley, S. Brumfield, A. F. Willis, Larissa Jackiw, M. Jutila, M. J. Young and T. Douglas, *J. Am. Chem. Soc.*, 2006, 128, 16626.
16. S. Takeda, M. Ohta, S. Ebina and K. Nagayama, *Biochim. Biophys. Acta*, 1993, 1174, 218.
17. H. Fukano, T. Takahashi, M. Aizawa and H. Yoshimura, *Inorg. Chem.*, 2011, 50, 6526.
18. T. Douglas and D. R. Ripoll, *Protein Sci.*, 1998, 7, 1083.
19. J. Heber, K. H. Hellwge, U. Köbler and H. Murmann, *Z. Physik*, 1970, 237, 189.